# Micro-Strain Distribution Around a Crack Tip by Electron Beam Moiré Methods

**Ouk Sub Lee* and David T. Read****

*(Received September 5, 1994)*

The microscopic deformation around a crack tip in a small tensile specimen of aluminum was measured by using electron beam moiré methods. The tensile test was carried out in a scanning electron microscope(SEM) by using specially designed small tensile testing apparatus for an SEM. A line grating with a pitch of 87 nm was written at the crack tip by electron beam lithography. SEM images of the grating contained(original) moiré fringes at certain magnifications without loadings on the specimen. The displacement and strain in the region 10 to 50 $\mu$ m from the crack tip were evaluated by analyzing the (mismatch) moiré fringes. Measured strains normal to loadings(longitudinal strains) near the crack tip were found to be comparable to those estimated using linear elastic fracture mechanics(LEFM), for the lowest load, and elastic-plastic fracture mechanics, at effective crack tip position located within the actual crack tip. The exponent of the strain singularity in the vicinity of the actual crack tip changed with applied stress, ranging between $-0.64$ and $-1.0$. The measured crack tip opening displacement(CTOD) values disagreed with CTODs based on the Hutchinson-Rice-Rosengren(HRR) field, the Dugdale model, and LEFM. The experimental plastic zones spread from the line of crack extension up to an angle of about 60°, as expected from LEFM theory.

**Key Words:** Dugdale Model, Elastic-Plastic Fracture Mechanics, Electron Beam Moiré, Gratings, HRR Singularity Field, LEFM, Lithography, Microcrack, Nanoscale Displacement, Plastic Zone, PMMA Resist, Scanning Electron Microscope, Strain, Stress Intensity Factor

## 1. Introduction

This paper describes an experimental study of the strain very near a crack tip in an aluminum tensile specimen. Because the highest strains, and therefore the initiation of cracking and failure, occur in the close vicinity of the crack tip, we are interested in the details of these strain fields as close as possible to the tip. Experimental studies of strain fields around crack tips and notch tips (Barker, 1985: Chiang, 1981: Cloud, 1992: Dally, 1991: Drinnon, 1992: Harresh, 1988: Kamath, 1990: Kang, 1987: Ke, 1973: Kobayashi, 1968: Liu, 1970: Mohajan, 1989: Nigam, 1988: Packman, 1975: Ramulu, 1983: Sciammarella, 1991: Theocaris, 1991: Tippur, 1991: Underwood, 1969) have been performed by a variety of techniques, mainly optical moiré, photoelasticity, and the methods of caustics. Most of these studies examined regions hundreds or thousands of micrometers away from the actual crack tip.

Spatial resolution of strain in geometrical moiré measurements is limited by the density of the grating written on the specimen and by the density and quality of the(virtual or physical) reference grating. Fringe multiplication techniques can extend the density of a grating. Such techniques lose contrast with increasing multiplication factor because the amplitude of the high-

* Mechanical Engineering Department Inha University, Inchon 402-751, Korea

** National Institute of Standard and Technology Materials Reliability Division 325 Broadway, Boulder Co 80303 U.S.A.

frequency components of the grating's contrast function decrease with increasing frequency. The spatial resolution of displacement remains limited by the pitch of the highest usable frequency component of the grating.

Optical techniques introduced by Post and others(Han, 1992 : McDonach, 1980 : Post, 1980 : Post, 1991) have produced gratings with a pitch of around 250 nm by optical interference. Moiré interferometry allows the formation of fringe images using selected higher diffraction orders from such gratings, increasing the effective line density by factors from 2 to 10 or more above the fundamental line density obtained by traditional optical techniques. In this technique, the physical reference grating of geometric moiré is replaced by a virtual grating produced by the interference of two beams of light. The gratings available in this technique are of sufficient quality that digital fringe multiplication has extended the precision of the displacement measurements by a factor of 10. However, the spatial resolution is limited by the magnification which can be used to obtain the images. Field sizes of 500 $\mu$m represent the limit of the current state of the art.

An alternative to optical interference is to produce line gratings by other lithography techniques. An electron beam lithography(Dally, 1993 : Haller, 1968 : Read, 1994) has been employed to produce a grating of 512 lines with a pitch of 87 nm. Examination of these gratings in the scanning electron microscope(SEM) produces moiré fringes because the raster scan pattern of the SEM serves as a virtual reference grating. Furthermore, the high magnifications available in the SEM allow highly localized observations of displacements.

In this paper the natural moiré fringes obtained when the pitch of the SEM raster nearly matches the pitch of the specimen grating were used. We were able to compare the theoretical and experimental strains in a region closer to the crack tip than has been reached heretofore. By considering both the magnitude and the spatial distribution of the strain, we were able to follow the transition from linear elastic fracture mechanics(LEFM) behavior to elastic-plastic fracture mechanics(EPFM) behavior. Considering the experimental error, we concluded that the LEFM and EPFM approximations which we employed gave an accurate estimate of the actual behavior of the strain field. The EPFM models for crack tip opening displacement(CTOD) did not apply well to our experimental situation, the measured displacement being larger than that predicted by the model. The switch from LEFM-like to EPFM-like behavior in our field of observation occurred at a nominal stress of $0.9\sigma_0$ where $\sigma_0$ is a reference yield yield stress(taken as 0.2 % offset yield stress in this paper).

## 2. Background

### 2.1 Experimental results on crack tip strain

A variety of experimental techniques, including photoelasticity, moiré , moiré with finite element methods(FEM), the methods of caustics, strain gages, laser speckle, and interferometry, have been used to investigate fracture phenomena in terms of stress intensity factor(SIF), energy release rate, and the J-integral, in various materials since the LEFM theory by Irwin(Irwin, 1958) and the EPFM theory known as Hutchinson-Rice-Rosengren(HRR) singularity fields by Hutchinson, and Rice and Rosengren(Hutchinson, 1968 : Rice, 1968) were published.

Most published experimental results describe behavior in regions a certain distance away from actual crack tips, according to the strengths and limitations of the individual techniques. The sizes of the fields covered by several experiments are listed in Table 1.

### 2.2 Crack tip strain fields

Our specimen had a very sharp crack, not a fatigue crack. The crack was so sharp and the plastic strains surrounding it so intense that the fracture mechanics theories are more appropriate for comparison than are theories for blunt notches. Furthermore, precedent for this approach is abundant in the literature, notably in(Dirnnen, 1992). Closed-form solutions for the strain fields around crack tips with some radii are available for the linear elastic case. A convenient

**Table 1** Extent of fields measured in previous studies of deformation near notch and crack tips

| Method | Measured quantity | Extent of field ($\mu$m from crack tip) | Ref. |
|---|---|---|---|
| Moiré | Displacement | 254 | (Underwood, 1969) |
| Moiré | Displacement | 1000 | (Kobayashi, 1968) |
| Moiré | Displacement | 1000 | (Liu, 1970) |
| Moiré | Displacement | 360 | (Ke, 1973) |
| Grid(powder) | Displacement | 140 | (Theocaris, 1991) |
| Computer-aided moiré | Displacement | 10 | (Sciammarella, 1991) |
| Moiré with photoelasticity | Displacement | 1000 | (Barker, 1985) |
| Grid moiré with strain gages | Displacement | 1000 | (Cloud, 1992) |
| Coherent gradient sensing | Displacement | 2250 | (Tippur, 1991) |
| Photoelasticity | Stress | 1300 | (Ramulu, 1983) |
| Photoelasticity | Stress | 2000 | (Dally, 1991) |
| Caustics with photoelasticity | Stress | 2000 | (Mohajan, 1989) |
| Caustics and photoelasticity | Stress | 2520 | (Nigam, 1968) |
| Moiré | Displacement | 158 | (Kang, 1987) |
| Moiré | Displacement | 1000 | (Drinnon, 1992) |
| Interferometry | Displacement | 80 | (Packman, 1975) |
| Moiré with FEM | Displacement | 1000 | (Hareesh, 1988) |
| White-light speckle | Displacement | 250 | (Chiang, 1981) |
| SIF tracer | SIF | 1250 | (Kamath, 1990) |

approximation for an actual crack tip with a radius is obtained(Creager, 1967) by calculating the strains as if the physical crack tip were located within the actual crack tip.

No exact closed-form solution is available for the strain at the tip of an elastic-plastic crack. However, the HRR(Hutchinson, 1968 : Rice, 1968) field gives graphically the behavior of a sharp crack in a power-law-hardening material. We used Creager's(Creager, 1967) approximation again for our elastic-plastic calculations.

It is important to note that no closed-form approximation to the whole strain field is applicable over the whole strain range, including both the elastic and elastic-plastic ranges. FEM are available, but these are influenced by the element type, element refinement, and material properties chosen, and give results only for specific sets of input values. Dugdale gave a model(Broek, 1982) that is useful for estimating CTOD, considering the effect of plasticity.

For the LEFM calculation, it is necessary to choose either a plane-stress or a plane-strain approach. Plane-strain would give strains about 10% higher than plane-stress, with the same form. The big difference between these idealizations is the size of the plastic zone. A plane-stress approximation was chosen in this study(Hutchinson, 1968 : Rice, 1968) ; this point is discussed further below, in light of the experimental results.

Elastic strains were calculated by using a very-near-field, plane-stress LEFM solution, which contains only the term of SIF. The theoretical strains $\varepsilon_{yy}$ along the $y$ direction are expressed as

$$\varepsilon_{yy}=\frac{K_I}{2\pi E\sqrt{r}}\cos\left(\frac{\theta}{2}\right)\left[(1-\nu)+(1+\nu)\sin\left(\frac{\theta}{2}\right)\sin\left(\frac{3\theta}{2}\right)\right] \quad (1)$$

where

$E$ is the elastic modulus,

$\nu$ is Poisson's ratio and

$r$ and $\theta$ are the local polar coordinates centered at the crack tip.

The classic EPFM description of the strain fields surrounding a crack tip is the HRR singularity. The asymptotic form of the plastic strains in the HRR singularity fields is given in terms of the stresses by(Hutchinson, 1968 : Rice, 1968)

$$\varepsilon_{yy}=\varepsilon_0\alpha\left[\frac{J}{\alpha\varepsilon_0\sigma_0 I_n r}\right]^{\frac{n}{n+1}}\tilde{\varepsilon}^{p}_{yy}(\theta,\ n) \quad (2)$$

where

$\varepsilon_o$ : $\sigma_o E$,

$\alpha$ : a constant in the Ramberg-Osgood model, here taken as 0.88,

$n$ : a constant in the Ramberg-Osgood model, here taken as 12,

$J$ : Rice's path-independent integral around the crack tip,

$I_n$ : a constant depending on $\alpha$ and $n$, here taken as 2.8,

$\sigma$ : remote applied stress,

$r$ : radial polar coordinate measured from the crack tip,

$\theta$ : angular polar coordinate measured from the crack propagation direction with origin at crack tip,

$a$ : crack length, and

$\tilde{\varepsilon}^{p}_{yy}(\theta,\ n)$ : angular dependence of the HRR strain field.

To obtain $J$ from our measured applied load, we use the usual relation between $J$ and $K$ for mode-I loading condition :

$$J=\alpha^{\frac{1}{n}}\frac{K_I^2}{E} \quad (3)$$

where

$K_I$ : the apparent SIF under mode-I loading.

No plastic zone corrections were used. For the elastic case, $\alpha=n=1$, we recover the familiar form $J_I=K_I^2/E$.

## 3. Specimen and Apparatus

The specimen material used in this measurement is a 5052-H32 aluminum alloy, with 0.2% offset yield stress $\sigma_o$, elastic modulus $E$, and Poisson's ratio $\nu$ of 174 MPa, 66 GPa, and 0.33, respectively. For calculations, below, the yield strain of the specimen material is taken as 0.00265. The two material constants for the power-hardening relation,

$$\frac{\varepsilon_{pl}}{\varepsilon_0}=\alpha\left(\frac{\sigma}{\sigma_0}\right)^n \quad (4)$$

were determined by fitting the stress-strain curve, as $\alpha=0.88$ and $n=12$, where $\sigma_o$ is a reference yield stress(taken as 0.2% offset yield stress in this paper). We took $\varepsilon_o=\sigma_o/E$.

The finished specimen was 1.12 mm thick and 4.2 mm wide in the gage length region. Figure 1 shows the specimen geometry and the material engineering stress-strain curve. A single edge crack 267 $\mu$m long and 10.1 $\mu$m wide at 5 $\mu$m behind the crack tip was introduced by applying very small loading with a new razor blade before the specimen surface was polished. The notch root radius was 6.2 $\mu$m.

A line grating was written at the notch tip using electron beam lithography. Applying polymethylmethacrylate(PMMA), which is used as an electron resist in lithography, causes a region of thick PMMA near the notch tip. Our grating was useful over a region from 5 to 30 $\mu$m from the end of the crack tip. The usable height of this grating was 45 $\mu$m. Its pitch was 87 nm, and it contained 512 lines.

A similar line grating is shown at a magnification of 60000 in Fig. 2. The scale bar representing 100 nm is visible. The dark regions represent trenches where the PMMA resist has been, first, damaged by exposure to the electron beam, and subsequently, dissolved by the developing solution. The light areas show ridges where the resist

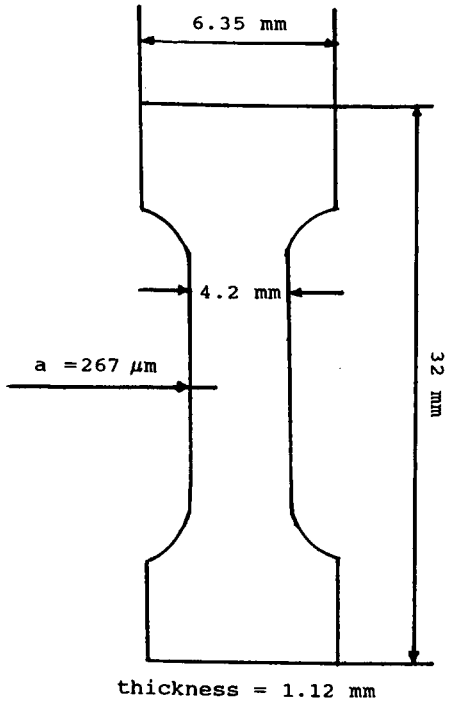


**Fig. 1** (a) Specimen geometry

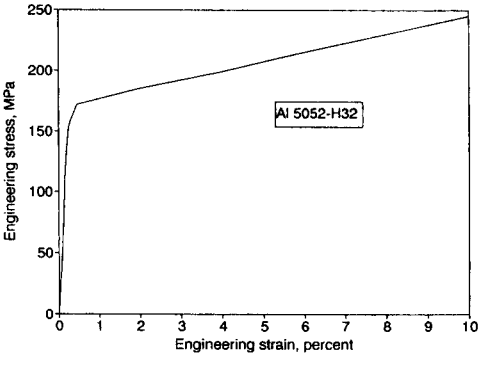


**Fig. 1** (b) Stress-strain curve of aluminum 5052-H32 specimen material

is intact. The trenches are about 10 nm wide, and the ridges are about 77 nm wide; this is equivalent to 11494 lines/mm. The electron dosages and the thickness of both PMMA resist and aluminum coating must be controlled carefully(Dally, 1993). The wandering lines in the grating of Fig. 2 result from wavy motion of the incident electron beam caused by electromagnetic interference and electronic noise in the microscope and by the random nature of electron backscattering. An 80 nm

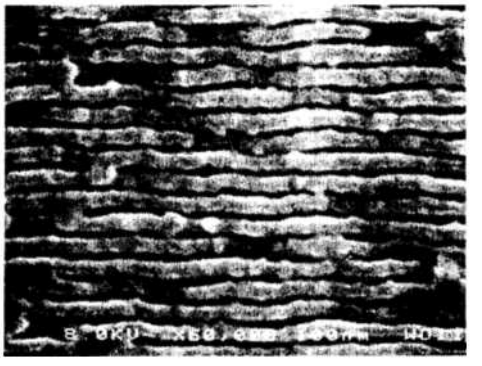

**Fig. 2** A typical line grating at a magnification of 60000

round shape randomly visible in the grating area was caused by nonuniform vacuum evaporation of the pure aluminum used to coat the specimen.

The specimen was mounted in a small tensile stage that fits into the chamber of the SEM. The tensile stage is equipped with clamped wedge grips. Both spur and worm gears are used to turn a pair of lead screws that drive both loading platens at equal rates. The applied load and platen displacement are measured with a load cell and LVDT(linear variable displacement transducer).

## 4. Electron Beam Moiré

In electron beam moiré method(Dally, 1993: Haller, 1968: Read, 1994), the raster scan pattern of the SEM acts as the reference grating. Moiré fringes are produced when a line grating is observed at appropriate magnification. The reference pitch can be varied by adjusting either the magnification of the SEM or the number of scan lines in the image. Figure 3 shows the grating used in this paper. The grating is 57 $\mu$m wide by 45 $\mu$m high.

The moiré fringes are mismatch fringes of division. Mismatch fringes of division are formed when

$$P_r = \beta P_s(1+\gamma) \tag{5}$$

where $P_s$ and $P_r$ are specimen grating pitch and reference grating pitch, $\beta$ is a fraction near unity, and $\gamma$ is an integer. In Fig. 3, the moiré fringes

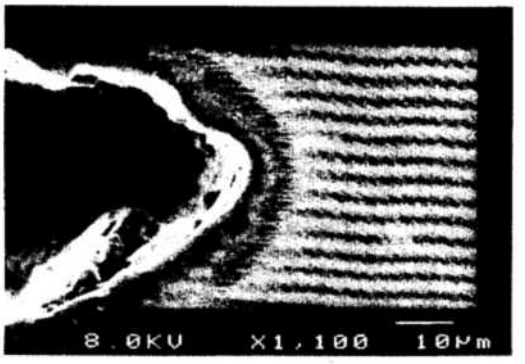


**Fig. 3** Electron beam moiré fringes of mismatch at magnification of 1100. Grating is 57 $\mu$m wide by 45 $\mu$m high

**Fig. 4** Electron beam moiré fringes arising from both mismatch and loading

shown are fringes of division, with $\gamma=1$. These fringes result from the slight mismatch between 2 $P_s$ and $P_r$. Here $P_s$ is 87 nm, while $P_r$, the pitch of the scan pattern of the SEM, is approximately 174 nm. The moiré fringes are clearly seen over most of the grating, except within about 5 $\mu$m the crack tip, where the specimen line grating is flawed because of significant variation of PMMA resist thickness. During the test, natural moiré fringes, where $P_s \approx P_r \approx 87$ nm, were recorded. A typical moiré fringe pattern resulting from both mismatch and loading is shown in Fig. 4.

## 5. Data Analysis and Results

### 5.1 Basic theory

The displacement in the longitudinal direction(normal to loadings) at load $P$ at any point in the image where $N_P$ is known as

$$V=N_P P_r \tag{6}$$

and the longitudinal strain(normal to loadings) any location in the field is

$$\varepsilon_{yy}=\frac{\partial V}{\partial y}=P_r\left(\frac{\partial N_P}{\partial y}-\frac{\partial N_0}{\partial y}\right) \tag{7}$$

where

$\varepsilon_{yy}$ is the strain along the tensile axis, normal to the reference grating lines,

$V$ is the displacement along the axis of the specimen and normal to the reference grating lines,

$P_r=76$ nm is the reference pitch at the SEM magnification of 2300,

$N_P(x, y)$ is the relative fringe order at position $x$, $y$ at load $P$, and

$N_o(x, y)$ is the relative fringe order at position $x$, $y$ before loading.

$x=r\cos\theta$, $y=r\sin\theta$.

$r$ and $\theta$ are the local polar coordinates centered at the crack tip.

In this paper $\partial N_0/\partial y$ is assumed to be constant over the grating area even though there are a few nonuniform mismatch moiré fringes, as shown in Fig. 4, because of imperfections in the specimen grating. Eq. (7) is thus written in a simpler manner as

$$\varepsilon_{yy}=\frac{\partial N_P}{\partial y}\times P_r-Constant \tag{8}$$

### 5.2 Displacement data acquisition

Moiré fringe images at various loads were obtained by acquiring SEM images at a slow scan rate of about 30 sec. per image and photographing a video display on the SEM. These photographs were converted to digital images using a video camera connected to a commercially available image-analysis system. The moiré fringes were traced on the video display using a manual tracking device.

In the image-analysis system, the loading direction was the $y$-direction. The crack was parallel to the $x$-axis. A series of locations for displacement and strain calculations was defined by, first, generating a set of 20 regularly spaced $y$-direction

lines across each image. Then, the image-analysis system reported the coordinates of the intersection of each of the traced fringes with each of these vertical lines. There were about 100 such intersections in each frame. Each intersection gives a value of the function $N_P(x, y)$.

Relative fringe numbers are sufficient to determine strains relative to the initial conditions of the test : in this case, the zero-load fringe pattern.

### 5.3 Displacement data fitting and estimation of strain values

Strain was estimated from the displacement. The displacements along each of the vertical lines were fitted to polynomials of varying degrees.

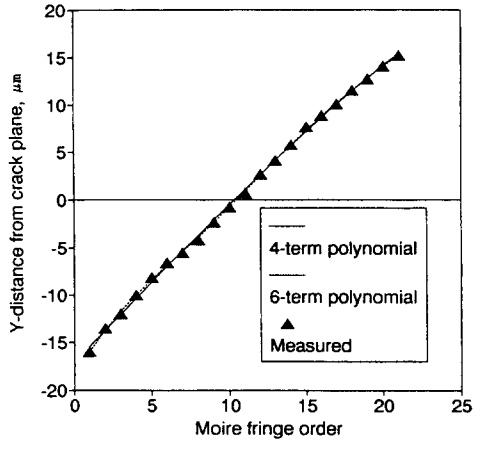


**Fig. 5** (a) Measured and numerically fitted displacement

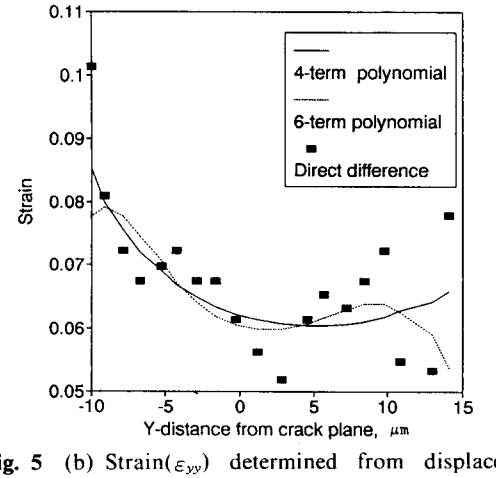


**Fig. 5** (b) Strain($\varepsilon_{yy}$) determined from displacement fits

These allowed interpolation of displacement values at all $y$-values along each of the vertical lines. Polynomials up to degree 5(6 terms) were tried. Figure 5(a) shows measured displacement data and fits made using polynomials of different degrees. Figure 5(a) shows that the fits to the measured displacements were little affected by the degree of the polynomial function used for the fit. A polynomial of degree 5 was chosen for analysis of all results in this paper.

Figure 5(b) shows strain distribution estimated using measured displacement(approximated with a polynomial of degree 5 as appeared) in Fig. 5(a).

## 6. Results and Discussion

An experimental strain distribution, along a line perpendicular to the crack face and 16 $\mu$m ahead of the crack tip, is shown in Fig. 6(a). (This line is only 10 $\mu$m ahead of the end of the actual crack. For consistency, all $x$-direction distances are measured relative to the theoretical crack tip.)

These data were obtained at a nominal stress level of $0.88\sigma_0$. The corresponding LEFM strain distribution is also shown, in Fig. 6. The $y$-

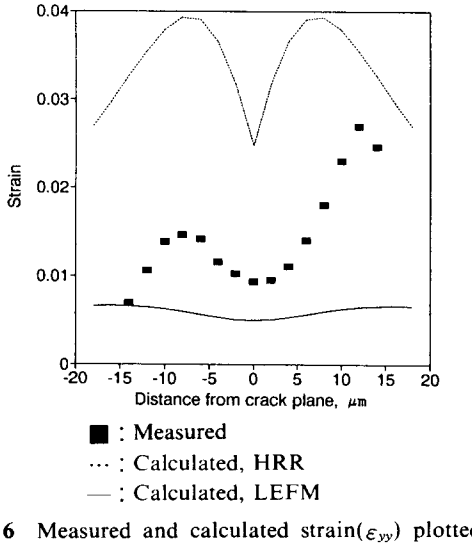


**Fig. 6** Measured and calculated strain($\varepsilon_{yy}$) plotted along a line perpendicular to the crack plane, 16 $\mu$m ahead of the theoretical crack tip and 10 $\mu$m ahead of the actual notch in the specimen

dependence of the experimental strain distribution appears to show the two peaks seen in the LEFM strain distribution, although the experimental strains are 2 to 6 times larger than the LEFM strains and the experimental strains are not symmetric about the plane of the notch. In Fig. 6 and all subsequent figures, $x$-direction distances are measured from the location of the theoretical crack tip, which is within the actual crack(Creager, 1967). The distance from the theoretical crack tip to the end of the actual crack was taken as 6.2 $\mu$m which adjust the position of the theoretical crack tip by allowing for the notch end radius of 6.2 $\mu$m; this value provided the best overall fit between the LEFM and EPFM calculations and the experimental strain data. Figure 6 also shows the HRR strain distribution ahead of the crack tip along the same line. The character of the variation of the strain is similar in the LEFM and HRR calculations, although the HRR value is much larger. The two peaks have moved closer in the HRR result. The experimental strain is intermediate in magnitude between the LEFM and HRR values. The locations of the peaks in the experimental strain are also intermediate between the LEFM and HRR locations. The experimental strain contains an asymmetry not present in either theory. Figures 7(a) and(b) show experimental strains near the notch tip at nominal stresses of 0.9 and 0.96$\sigma_o$ as isometric strain contours.

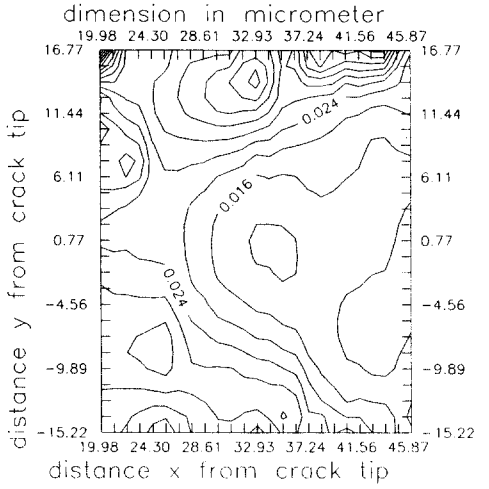


(a) 0.90$\sigma_o$

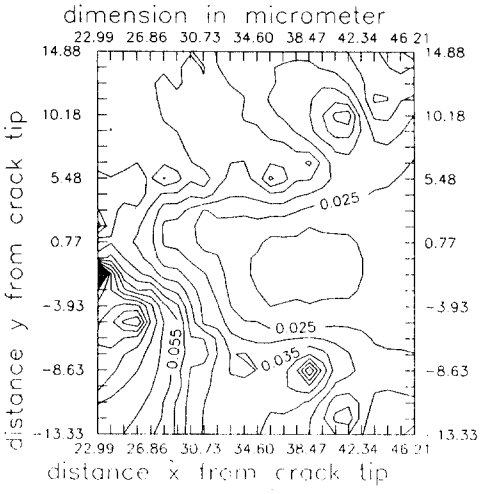


(b) 0.96$\sigma_o$

**Fig. 7** Isometric strain($\varepsilon_{yy}$) contours at two load levels

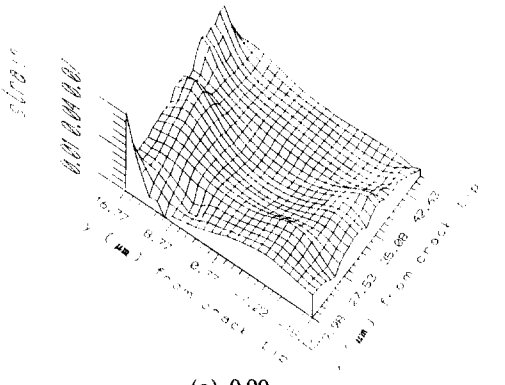

(a) 0.90$\sigma_o$

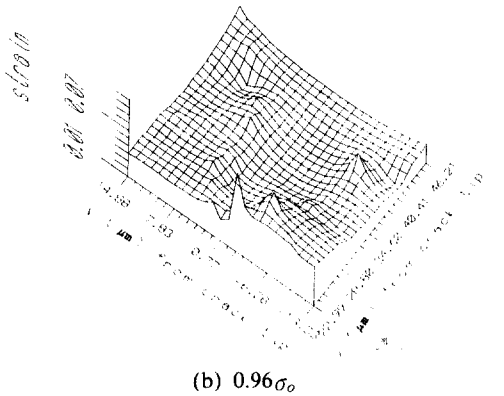

(b) 0.96$\sigma_o$

**Fig. 8** Three-dimensional view of isometric strain($\varepsilon_{yy}$) at two loads

Three-dimensional views are given in Figs. 8(a) and(b).

The configurations of these contours of constant longitudinal strain $\varepsilon_{yy}$ differ from some previous observations, but are similar to others. For example, the results of Fig. 7 are different from those measured macroscopically by the conventional moiré method for a region about 2000 $\mu$ m from the crack tip and beyond in a centrally notched magnesium plate under uniaxial tensile loading(Kobayashi, 1967). However, Fig. 7 is in qualitative agreement with the contours of constant $\varepsilon_{yy}$ at the crack tip obtained by using a computer vision method(Sutton, 1992). The region of lower strain surrounded by higher strains may be related to a reduced deviatoric stress(Liu, 1984).

The electron beam moiré fringe patterns from which the data of Figs. 7 and 8 were taken are shown in Fig. 9.

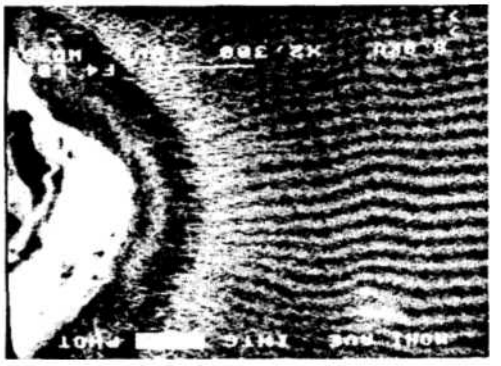

(a) $0.90\sigma_o$

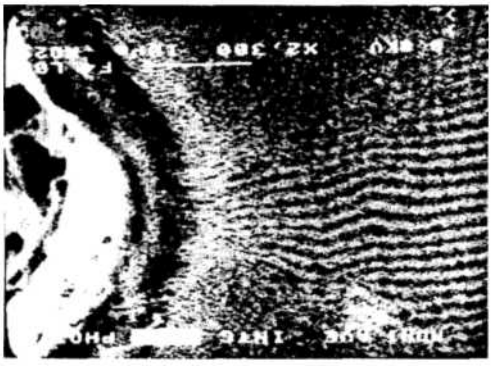

(b) $0.96\sigma_o$

**Fig. 9** Electron beam moiré fringe patterns at two loads

The configuration of the moiré fringe patterns ahead of the actual crack tip looks more like that of a stressed region near a hole than like that of a crack tip(Post, 1983). However, the experimental strains along the line of crack extension reach 15 times the reference yield strain $\varepsilon_o$, as shown in Fig. 10(a).

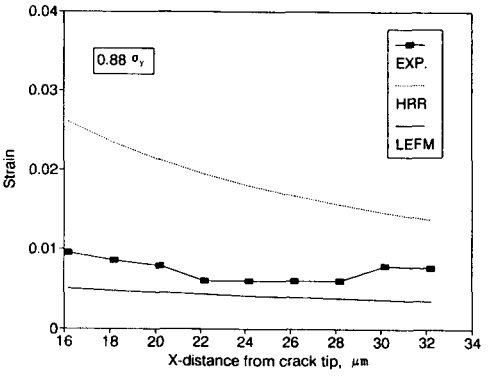


(a) $0.88\sigma_o$

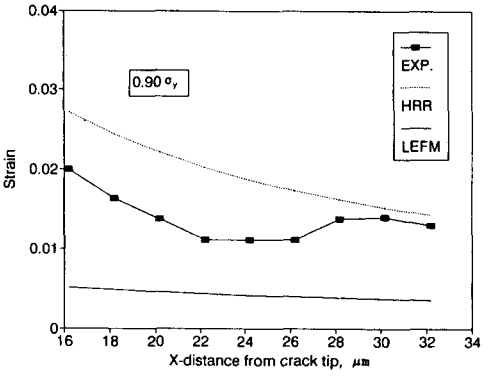


(b) $0.90\sigma_o$

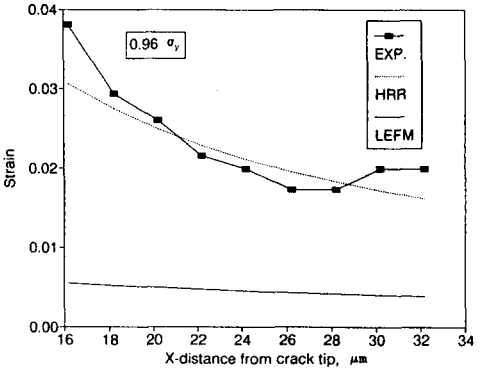


(c) $0.96\sigma_o$

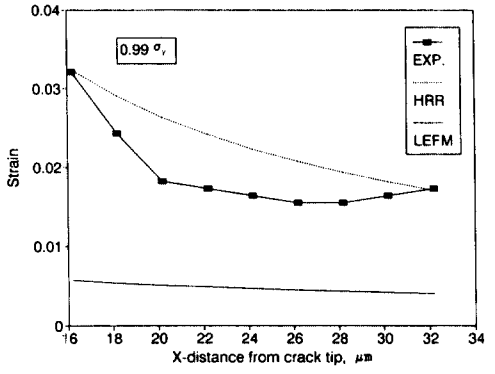


(d) $0.99\sigma_o$

**Fig. 10** Measured longitudinal strain($\varepsilon_{yy}$), strain calculated using LEFM and strain calculated using EPFM, plotted against distance from the theoretical crack tip, along the crack line(Y=0). Applied stresses are indicated as fractions of the yield strength

loads were estimated by fitting a singular term to the data. Strain singularities ranging from $-0.64$ to $-1.0$ are found, Fig. 11.

These nearly match the range from the LEFM

Experimental strain distributions along the line of crack extension, corresponding to four different applied loads, are shown in Figs. 10(a~d). Figure 10 also shows theoretical strain distributions calculated using LEFM theory and HRR fields. As discussed above, for calculation, the theoretical crack tip is offset from the actual crack tip by

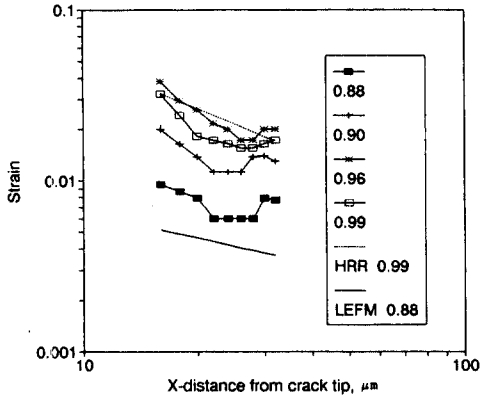


**Fig. 11** Logarithmic plot of theoretical extreme strains($\varepsilon_{yy}$) and experimental strains($\varepsilon_{yy}$) at four different loads, plotted against distance from the crack tip

an amount equal to the notch tip radius, 6.2 $\mu$m, and $x$-distances are measured from the theoretical crack tip.

The two key features of $\varepsilon_{yy}$ along the crack propagation direction are its magnitude and its rate of decay with distance from the crack tip. A general overview of Fig. 10 indicates that the measured strains are in the wide range between the LEFM and EPFM theories and that their rate of decay with distance from the crack tip is generally similar to the theoretical results. Figure 10(a) shows that the measured strains are closer to the LEFM calculation for a load of $\sigma/\sigma_o=0.88$. Figures 10(b~d) show that the measured strains are closer to the HRR calculation than to the LEFM values at the higher load($\sigma/\sigma_0 \geq 0.9$).

Similar results have been reported before, for regions much further from the crack tip than those covered in the present study. For example, Drinnon and Kobayashi(Drinnon, 1992) reported agreement between experimental strains and the HRR field after adjusting their crack tip position. They studied a region about 3000 $\mu$m from the crack tip. Furthermore, under a lower load condition, $\sigma/\sigma_o=0.88$, their experimental strains agreed better with LEFM calculations. Ke and Liu(Ke, 1973) found agreement between their measurements and LEFM for a region about 360 $\mu$m from the crack tip and beyond, under a lower load $\sigma/\sigma_o=0.25$.

The orders of the strain singularities characteristic of the experimental strains under varying value of $-0.5$ to the HRR value of $-0.93$ for our material's strain hardening.

There are regions in the experimental records where no moiré fringes were visible because the grating pulled away from the specimen as the load increased. These regions have strains larger than 0.017, which was the highest measurable strain, and are considered to be part of the apparent plastic zone. These zones spread out from the crack tip at angles of about $\pm 60°$ from the crack line ; the shape resembled one estimated by EPFM(Knott, 1973). The 60° angle was confirmed after the test by optical examination, Fig. 12.

The plastic zone diameter $d_y$ can be estimated


**Fig. 12** Optical micrograph of the shape of the apparent plastic zone near the end of the notch

by LEFM theory for plane-stress(Broek, 1989) :

$$d_y=\left(\frac{K_I}{\sigma_0}\right)^2\frac{1}{\pi} \tag{9}$$

where

$K_I$ is the mode-I SIF and

$\sigma_o$ is a reference yield stress under uniaxial loads(taken as 0.2% offset yield stress).

For the stress studied, the calculated plastic zone sizes for plane-stress are 260, 276, 316 and 336 $\mu$m, corresponding to applied apparent SIF $K_I$ of 4.98, 5.12, 5.48, and 5.65 MPa$\sqrt{\text{m}}$. The plastic zone sizes under plane-strain conditions are 29, 31, 35 and 37 $\mu$m. In applying these calculations to the experiment, we consider that the theoretical crack tip is located within the actual crack(Creager, 1967). The plane-stress plastic zones are much larger than the moiré grating. For the lowest stress, the plane-strain plastic zone extends from the theoretical crack tip to about the middle of the grating. Figure 10 shows that the strain at the lowest load is above, but near, LEFM values, while at higher loads the strain is far above the LEFM values and at the highest load approaches the EPFM values. The measured strains for the stress level of 0.96 $\sigma_o$ exceed 7 times the yield strain throughout the grating. However, the LEFM-calculated plastic zone size for this case, for plane strain, would put the edge of the plastic zone within the grating. From these results, we conclude that the plane-strain approximation is better at 0.88 $\sigma_o$, but that by 0.96 $\sigma_o$, the triaxiality has broken down, and plane stress is the better approximation.

The CTOD in this experiment was taken as the increase of the notch width over its value at zero load. The CTODs at 5 $\mu$m behind the actual crack tip are plotted against $J$-integral in Fig. 13.

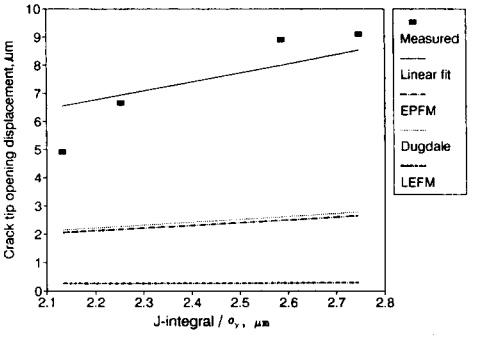


**Fig. 13** CTOD estimated by various theoretical models, compared to measured values. The quantity $J/\sigma_o$ plotted on the x-axis is nearly proportional to the square of the applied stress

The $J$-integrals were obtained from the applied loads using Eq. (3). The measured CTODs appear to be nearly proportional to the $J$-integral. The experimental proportionality constant $d_n$ in the EPFM formula CTOD$=d_nJ/\sigma_o$ is about 3 ; this is found to be much different from the theoretical value of 1 or less, based on HRR field theory. It seems that the approximation of our actual blunt-ended crack to the theoretically sharp crack considered in EPFM fails to predict realistic values for CTOD.

## 7. Conclusions

Electron beam moiré has been applied to a classic problem in experimental mechanics : crack

tip deformation. A line grating with a pitch of 87 nm, corresponding to a density of 11494 lines/mm, was placed at the tip of a notch with an end radius of 6.2 $\mu$m Deformation and strain($\varepsilon_{yy}$) were measured from 5 to 30 $\mu$m from the notch end. The experimental strain distribution along the line of crack extension was found to be consistent with LEFM at lower loads, and with the HRR singularity at higher loads, after adjusting the position of the theoretical crack tip to allow for the notch end radius of 6.2 $\mu$m. The main results are the followings : 1) The orders of strain singularity varied from $-0.64$ to $-1.0$ with applied load levels. The value of $-1.0$ is in approximate agreement with the theoretical HRR singularity of $-0.93$, which is independent of load. 2) The available EPFM models for CTOD did not apply to the present experimental situation : the models predict CTOD much lower than the values derived from experiment. 3) The apparent plastic zones at the notch end spread out with angles about 60 degree to the crack propagation line and resembled the LEFM estimate.

## Acknowledgment

The first author wish to acknowledges the financial support from the Education Ministry of Korea during this investigation.

## References

Barker, D. B., Sanford, R. J. and Chona, R., 1985, "Determining K and Related Stress-Field Parameters from Displacement Fields," *Experimental Mechanics*, Vol. 25, No. 4, pp. 399~407.

Broek, D., 1982, Elementary Engineering Fracture Mechanics, Martinus Nijhoff, The Hague, p. 94.

Broek, D., 1989, "The Practical Use of Fracture Mechanics," Kluwer Academic Publishers, Boston, pp. 31~66.

Chiang, F. P. and Asundi, A., 1981, "A White Light Speckle Method to the Determination of Stress Intensity Factor and Displacement Field around a Crack Tip," *Engineering Fracture Mechanics*, Vol. 15, No. 1-2, pp. 115~121.

Cloud, G. L. and Paleebut, S., 1992, "Surface and Interior Strain Fields Measured by Multiple-Embedded-Grid Moiré and Strain Gages," *Experimental Mechanics*, Vol. 32, No. 3, pp. 273~281.

Creager, M. and Paris, P. C., 1967, "Elastic Field Equation for Blunt Cracks with Reference to Stress Corrosion Cracking," *International Journal of Fracture*, Vol. 3, pp. 247~252.

Dally, J. W. and Riley, W. F., 1991, Experimental Stress Analysis, McGraw-Hill, Inc. p. 508.

Dally, J. W. and Read, D. T., 1993, "Electron Beam Moiré," *Experimental Mechanics*, Vol. 33, No. 4, pp. 270~277.

Drinnon, R. H. and Kobayashi, A. S., 1992, "J-Intergral and HRR Field Associated with Large Crack Extension," *Engineering Fracture Mechanics*, Vol. 41, No. 5, pp. 685~694.

Haller, I., Hatzakis, M. and Srinivasan, R., 1968 "High Resolution Positive Resist for Electron-Beam Exposure," *IBM Journal Research and Development*, Vol. 12, pp. 251~256.

Han, B., Lim, C. K., Guo, Y. and Post, D., 1992, "Thermal Deformation Analysis for Interconnections in Electronics Packaging by Microscopic Moiré Interferometry," 1992 SEM Ⅶ International Congress on Experimental Mechanics, Las Vegas, Nevada, pp. 442~448.

Hareesh, T. V. and Chiang, F. P., 1988, "Integrated Experimental-Finite Element Approach for Studying Elasto-Plastic Crack Tip Fields," *Engineering Fracture Mechanics*, Vol. 31, No. 3, pp. 451~461.

Hutchinson, J. W., 1968, "Plastic Stress and Strain Field at a Crack Tip," *Journal of Mechanics and Physics of Solids*, Vol. 16, pp. 337~347.

Irwin, G. R., 1958, "Fracture," Handbuch der Physik, Springer Verlag, Berlin, Vol. 6, p. 551.

Kamath, S. M. and Kim, K. S., 1990, "On Measuring the Near Tip Plastic Strain Singularity," *Journal of Applied Mechanics*, Vol. 57, pp. 901~905.

Kang, B. S.-J., Kobayashi, A. S. and Post, D., 1987 "Stable Crack Growth in Aluminum Tensile

Specimens," *Experimental Mechanics*, Vol. 27, No. 3, pp. 234~245.

Ke, J. S. and Liu, H. W., 1973, "The Measurement of Fracture Toughness of Ductile Mate-

McDonach, A., McKelvie, J. and Walker, C. A., 1980, "Stress Analysis of Fibrous Composites Using Moiré Interferometry," *Optics and Laser Engineering*, Vol. 1, pp. 85~105.

Mohajan, R. V. and Ravi-Chandar, K., 1989, "Experimental Determination of Stress Intensity Factors Using Caustics and Photoelasticity," *Experimental Mechanics*, Vol. 29, No. 1, pp. 6~11.

Nakamura, T. and Parks, D. M., 1988, "Three Dimensional Stress Field Near the Crack Front of a Thin Elastic Plate," *Journal of Applied Mechanics*, Vol. 55, pp. 805~813.

Nigam, H. and Shukla, A., 1988, "Comparison of the Techniques of Transmitted Caustics and Photoelasticity as Applied to Fracture," *Experimental Mechanics*, Vol. 28, No. 2, pp. 123~135.

Packman, P. F., 1975, "The Role of Interferometry in Fracture Studies," Experimental Techniques in Fracture Mechanics, Society of Experimental Mechanics Monograph No. 2, Edited by A. S. Kobayashi, The Iowa State University Press, pp. 59~87.

Post, D., 1980, "Optical Interference for Deformation Measurement-Classical, Holographic and Moiré Interferometry," Mechanics of Nondestructive Testing, W. W. Stinchcomb, ed., Plenum Press, New York, pp. 1~53.

Post, D., Czarnek, R. and Smith, C. W., 1983, "Patterns of U and V Displacement around Cracks in Aluminum by Moiré Interferometry," Proceedings of Int. Conf. on Application of Fracture Mechanics to Materials and Structures, Freiburg, F. R. G., June 20~24, pp. 699~708.

Post, D., 1991, "Moiré Interferometry: Advances and Applications," *Experimental Mechanics*, Vol. 31, No. 3, pp. 276~280.

Ramulu, M. and Kobayashi, A. S., 1983, "Dynamic Crack Curving-A Photoelastic Evaluation," *Experimental Mechanics*, Vol. 23, No. 1, pp. 1~9.

Read, D. T. and Dally, J. W., "Electron Beam Moiré Study of Fracture of a GFRP Composite," to be Published, *Journal of Applied Mechanics*.

Rice, J. R. and Rosengren, G. F., 1968, "Plane Strain Deformation Near a Crack Tip in a Power-Law Hardening Material," *Journal of*

rials," *Engineering Fracture Mechanics*, Vol. 5, pp. 187~202.

Knott, J. F., 1973, *Fundamentals of Fracture Mechanics, Butterworths*, pp. 30~79.

Kobayashi, A. S., Harris, D. O. and Engstrom, W. L., 1967, "Transient Analysis in a Fracturing Magnesium Plate," *Experimental Mechanics*, Vol. 7, No. 10, pp. 434~440.

Kobayashi, A. S. and Engstrom, W. L., 1968 "Transient Analysis in a Fracturing Aluminum Plate," Office of Naval Research Contract Nomr-477 NR064, 478.

Liu, H. W., Gavigan, W. J. and Ke, J. S., 1970, "An Engineering Analysis of Ductile Fracture," *International Journal of Fracture Mechanics*, Vol. 6, No. 1.

Liu, H. W. and Zhuang, T., 1984, "Characteristic Crack Tip Field and the Charaterizing Parameters for Elastic-Plastic Fracture Mechanics," Advances in Fracture Research(Fracture84, ICF6), pp. 777~790.

*Mechanics and Physics of Solids*, Vol. 16, pp. 1~12.

Sciammarella, C. A. and Bhat, G., "High Resolution Computer-Aided Moiré," SPIE Vol. 1554B, Moiré Techniques, Holographic Interferometry, Optical NDT and Application to Fluid Mechanics, pp. 162~173.

Sutton, M. A., Turner, J. L., Chao, Y. J., Bruck, H. A. and Chae, T. L., 1992, "Experimental Investigation of Three-Dimensional Effects Near a Crack Tip using Computer Vision," *International Journal of Fracture*, Vol. 53, pp. 201~228.

Theocaris, P. S., 1991, "The Elastic Field around the Crack Tip Measured by Scanning Electromicroscopy," *Engineering Fracture Mechanics*, Vol. 37, No. 4, pp. 739~751.

Tippur, H. V. and Rosakis, A. J., 1991, "Quasi-Static and Dynamic Crack Growth along Bimaterial Interfaces: A Note on Crack Tip Field Measurements using Coherent Gradient Sensing," *Experimental Mechanics*, Vol. 31, No. 3, pp. 243

~251.

Underwood, J. H. and Kendall, D. P., 1969, "Measurement of Micro-scopic Plastic Strain Distribution in the Region of a Crack Tip," *Experimental Mechanics*, Vol. 9, No. 7, pp. 296~304.